J Arid Land (2023) 15(4): 439–459
https://doi.org/10.1007/s40333-023-0098-0

Science Press Springer-Verlag

Temporal and spatial variation characteristics of extreme precipitation on the Loess Plateau of China facing the precipitation process

ZHANG Yixin[1], LI Peng[1*], XU Guoce[1], MIN Zhiqiang[2], LI Qingshun[2], LI Zhanbin[1,3], WANG Bin[1], CHEN Yiting[1]

[1] State Key Laboratory of Eco-Hydraulic in Northwest Arid Region, Xi'an University of Technology, Xi'an 710048, China;
[2] Key Laboratory of National Forestry and Grassland Administration on Ecological Hydrology and Disaster Prevention in Arid Regions, Northwest Survey and Planning Institute of National Forestry and Grassland Administration, Xi'an 710048, China;
[3] State Key Laboratory of Soil Erosion and Dryland Farming on the Loess Plateau, Chinese Academy of Sciences and Ministry of Water Resources, Yangling 712100, China

Abstract: The preceding and succeeding precipitation (PSP) often act together with extreme precipitation (EP), in turn, causing floods, which is an objective component that is often overlooked with regard to summer flood hazards in the arid region of Northwest China. In this study, event-based extreme precipitation (EEP) was defined as continuous precipitation that includes at least one day of EP. We analyzed the spatiotemporal variation characteristics of four EEP types (front EEP, late EEP, balanced EEP, and single day EEP) across the Loess Plateau (LP) based on data acquired from 87 meteorological stations from 1960 to 2019. Precipitation on the LP basically maintained a spatial pattern of "low in the northwest region and high in the southeast region", and EP over the last 10 a increased significantly. The cumulative precipitation percentage of single day EEP was 34% and was dominant for 60 a, while the cumulative precipitation percentage of front, late, and balanced EEP types associated with PSP accounted for 66%, which confirms to the connotation of EEP. The cumulative frequencies of front and late EEP types were 23% and 21%, respectively, while the cumulative frequency of balanced EEP had the lowest value at only 13%. Moreover, global warming could lead to more single day EEP across the LP, and continuous EEP could increase in the northwestern region and decrease in the eastern region in the future. The concept of process-oriented EP could facilitate further exploration of disaster-causing processes associated with different types of EP, and provide a theoretical basis for deriving precipitation disaster chains and construction of disaster cluster characteristics.

Keywords: temporal and spatial variation; climate change; extreme precipitation (EP); event-based extreme precipitation (EEP); Loess Plateau

Citation: ZHANG Yixin, LI Peng, XU Guoce, MIN Zhiqiang, LI Qingshun, LI Zhanbin, WANG Bin, CHEN Yiting. 2023. Temporal and spatial variation characteristics of extreme precipitation on the Loess Plateau of China facing the precipitation process. Journal of Arid Land, 15(4): 439–459. https://doi.org/10.1007/s40333-023-0098-0

1 Introduction

1.1 Impact of global climate change on extreme precipitation (EP)

According to the Intergovernmental Panel on Climate Change (IPCC) Sixth Assessment Report (AR6), extreme climate has been discussed in a separate chapter, and a comprehensive and

*Corresponding author: LI Peng (E-mail: lipeng74@163.com)
Received 2022-06-08; revised 2022-09-22; accepted 2022-10-05

systematic assessment of changes in extreme climate events has been carried out for the first time (IPCC, 2021). AR6 focuses on the event trends at regional scale under various warming levels, and has made some progress in the attribution of single and unit events and compound events when compared to the IPCC Fifth Assessment Report (IPCC, 2014). An important consequence of the rising global temperatures is that the atmosphere will hold more water vapor, resulting in considerably stronger and more frequent heavy precipitation events in some regions (Aihaiti et al., 2021; Yang et al., 2022). With the intensification of global warming, variation in regional heavy precipitation intensities at the global scale exhibits a near linear relationship with the magnitude of global warming. For every 1°C increase in global temperature in the future, the intensity of extreme daily precipitation events is likely to increase by 7% (P<0.05) (Sillmann et al., 2013; Donat et al., 2016; Yao et al., 2020). The risk of heavy precipitation, which is considerably influenced by the westerly circulation and a typical semi-arid continental monsoon climate in arid regions, such as the Loess Plateau (LP) in mid-latitude Asia, has increased (Li et al., 1988; Donat et al., 2019). The average temperature on the LP during 1961–2010 has increased by nearly 2°C, with the increase exceeding the average temperature increase in China, which is a sensitive subject with regard to climate change (Peterse et al., 2011; Miao et al., 2016; Wu et al., 2019; Liu and Wu, 2021). Numerous studies have shown that the variation trend of annual precipitation on the LP is almost insignificant, although the annual precipitation intensity has exhibited a significant increasing trend over the past few decades (Gao et al., 2015; Sun and Ma, 2015). However, the internal geomorphological environment of the LP is complex, and researchers usually divide the LP into several major subregions based on the geomorphological types; therefore, certain climate change indices associated with the LP are highly heterogeneous and temporally inhomogeneous (Zhao et al., 2018).

1.2 Research perspectives of EP

Studies have shown that more than 90% of natural disasters are caused by extreme climate events. Owing to the unique geology and topography of the LP, the intense water erosion area (soil erosion modulus≥8000 t/(km^2·a)) is 85,100 km^2, accounting for 64% of the total area under this category in China, the severe water erosion area (soil erosion modulus≥15,000 t/(km^2·a)) is 36,700 km^2, accounting for 89% of the total area under this category in China, and the erosion modulus in some areas exceeds 30,000 t/(km^2·a) (Gao et al., 2018). Despite the large-scale ecological construction on the LP since 1980, which has significantly reduced sediment transport, the typical tributaries of the Yellow River still maintain a high level of sediment load under extreme precipitation (EP). Similarly, gully erosion, terrace- and dam-induced erosion, and decline in farmland fertility occur frequently, thereby having a direct and severe impact on the ecological environment and social and economic development (Jin et al., 2021). With regard to research on soil erosion processes and disasters on the LP caused by EP, a few studies have highlighted two key issues: the macro and micro characteristics associated with the development of heavy rain and soil erosion processes (Wang et al., 2022; Yang et al., 2022). The present study focused mainly on the EP process, which is a further analysis based on precipitation indicators. The process-oriented studies of precipitation events have been conducted in the northern highlands of Pakistan and the Qinling Mountains of China (Li et al., 2020; Zaman et al., 2020). Therefore, it is necessary to carry out similar studies on the LP to enhance our understanding of EP processes and associated disasters, and provide baseline information that could guide the ecological construction of key areas on the LP.

A precipitation event is a two-dimensional process consisting of precipitation amount and time. The event usually occurs in three stages based on time dimension: initial, development, and decay stages, and the entire process may last from a few hours to a few days (White et al., 2017). Event-based extreme precipitation (EEP) can be divided into EP and preceding and succeeding precipitation (PSP) (Hitchens et al., 2013). In most studies of EP, researchers explored the trend, frequency, and probability of a certain threshold event by statistical analyses based on different time and spatial scales. The PSP and EP are usually regarded as separate parts (Xiao et al., 2016;

Wang et al., 2019). Datasets from certain areas show that EP causes high-level precipitation; however, PSP should be taken into account, especially in areas that experience a humid monsoon climate (Ding et al., 2020). Although PSP does not reach a threshold on a daily scale, its accumulation is likely to aggravate runoff in local areas and prolong the flood duration, leading to catastrophic floods (Hamidreza et al., 2010; Fu et al., 2020). For example, during the heavy precipitation event that struck the Yellow River Basin of China from 26 July to 28 July in 2017, the cumulative precipitation of the event was approximately 160.0 mm, with the precipitation observed on 26 July, 27 July, and 28 July being 91.5, 35.6, and 32.8 mm, respectively. The precipitation observed on 26 July 2017 (91.5 mm) is presumed to have reached a daily standard heavy precipitation threshold (>50.0 mm), whereas precipitation observed on the other two days (35.6 and 32.8 mm) was categorized as PSP, which is below the statistical standard and cannot be considered extreme. Nevertheless, PSP in such an event may also exacerbate flooding disasters as previously reported (Jin et al., 2018; Yao et al., 2018; Guo et al., 2019; Wang et al., 2020). PSP is more frequent in certain areas that receive continuous precipitation, such as southeastern China, which belongs to the subtropical highs and is influenced by the equatorial southeast monsoon weather in summer, with long-lasting precipitation (Hu et al., 2011). If EP under a certain threshold is considered separately, without taking PSP into account, the impact of EP aggregation on local runoff on a daily scale may be underestimated. To date, the time distribution pattern of EEP, which is also referred to as the temporal profile, remains highly uncertain and intractable (Back et al., 2011; Ghassabi et al., 2016). However, researchers have reached a consensus that treating EP as a continuous and complete event, in addition to identifying the time position of EP in the entire precipitation process and evaluating the type of time profile pattern corresponding to the precipitation process can better define EP (Caballero and Rahman, 2013; Wu et al., 2018; Zaman et al., 2020). On the basis of daily-scale trend analysis, a combination of the method with the time profile of the process can compensate for the absolute threshold or relative range of precipitation, which is consistent with the essential characteristics of the continuity and periodicity of precipitation (Li, et al., 2020). Therefore, this study introduced the concept of EEP, extracted EEP data, and then inquired the time profile of the precipitation process, in addition to categorizing EEP to take the variations in EP on the LP into consideration. The results of this study could enhance our understanding of the EP events on the LP, and provide a theoretical basis for improving regional comprehensive risk management.

2 Materials and methods

2.1 Study area

The LP (103.5–114.5°E, 32.5–42.5°N) is one of the four major plateaus in China, with a total area of 6.35×10^5 km^2 and an altitude of 100–5225 m (Fig. 1). The LP is the second echelon of China's topography with a variety of landforms, including hills, high plateaus, desert plains, arid grasslands, highland grasslands, and earth-rock mountains. The annual average temperature is 3.6°C–14.3°C and the average annual precipitation is 150.0–750.0 mm, which mainly occurs from June to September, with considerable intra- and inter-annual changes, as well as the same period of precipitation and heat (Wang et al., 2021). The vegetation on the LP, which is influenced by altitude and topography, transits gradually from the forest and steppe to typical steppe and desert steppe from the southeastern region to the northwestern region, thereby exhibiting a zonal distribution pattern. According to the previous study (Yang et al., 2019), we classified the LP into four zones based on the topography and landforms: northern aeolian sandy agricultural irrigation area (Zone I), hilly and gully area (Zone II), plateau and gully area (Zone III), and eastern river valley and rocky mountainous area (Zone IV).

2.2 Data sources

The daily precipitation datasets of 87 meteorological stations on the LP and its surrounding areas were obtained from the China Meteorological Data Service Centre (http://data.cma.cn). In order

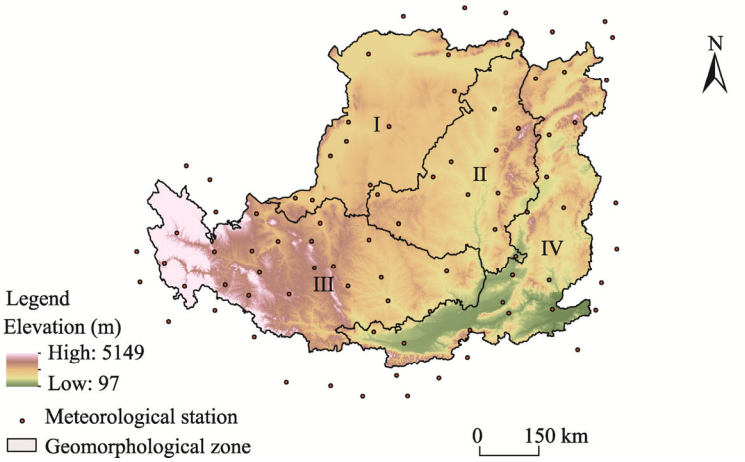

Fig. 1 Overview of the study area and spatial distribution of the four geomorphological zones. Zone I, northern aeolian sandy agricultural irrigation area; Zone II, hilly and gully area; Zone III, plateau and gully area; Zone IV, eastern river valley and rocky mountainous area.

to ensure the integrity and continuity of the dataset, we set the study period from 1960 to 2019. Short-term missing data at a single station were interpolated using the mean value of precipitation at adjacent stations. The quality inspection of the dataset was tested by Relative Homogenization test (RHtest) (Wang et al., 2010).

2.3 Data analysis

2.3.1 EP indices

In this study, we selected five indices based on the EP indices recommended by the Expert Team on Climate Change Detection and Indices (ETCCDI) and a comprehensive consideration of their definitions (Malinovic et al., 2016; Guo et al., 2019). In addition, erosive precipitation (≥12.0 mm) on the LP has a major impact on rainstorm erosion (Liu et al., 2018). Therefore, we selected seven EP indices, including annual total wet-day precipitation (PRCPTOT), annual total erosive precipitation (R12TOT), annual total extreme heavy precipitation (R50TOT), wet days (Pday), total precipitation on very wet days (90pTOT), wet days in flood season (FSPday), and simple precipitation intensity index (SDII) (Table 1).

Table 1 Definition of extreme precipitation (EP) indices used in this study

Index	Definition	Unit
Annual total wet-day precipitation (PRCPTOT)	Sum of annual precipitation	mm
Annual total erosive precipitation (R12TOT)	Sum of precipitation≥12.0 mm	mm
Annual total extreme heavy precipitation (R50TOT)	Sum of precipitation≥50.0 mm	mm
Total precipitation on very wet days (90pTOT)	Sum of precipitation with daily precipitation≥90^{th} percentile	mm
Wet days (Pday)	Sum of annual precipitation days	d
Wet days in flood season (FSPday)	Sum of precipitation days in flood season	d
Simple precipitation intensity index (SDII)	Average precipitation in precipitation days	mm/d

2.3.2 Event-based extreme precipitation (EEP) definition and classification

Variations in the location and amount of EEP may lead to variations in hazards and their effects. The definition and classification of EEP types are based on relevant theories (Wu et al., 2018). The main steps are as follows (Fig. 2): firstly, if the daily precipitation is continuous (daily precipitation≥1.0 mm for several consecutive days), a continuous effective precipitation event is extracted; secondly, if a valid continuous precipitation event includes EP (daily precipitation≥the 90^{th} percentile in the continuous precipitation series), it is upgraded to an EEP; thirdly, based on

the location attributes of EP in EEP events, the EEP types are mainly classified into four categories, including front EEP (EP becomes intense during the first half of the total precipitation period; no EP is observed during the later period, which is coupled with a concomitant decrease in intensity), late EEP (precipitation is weak over the first half of the precipitation period and no EP is observed; EP becomes intense during the second half of the total precipitation period), balanced EEP (EP is distributed during both the front and late precipitation periods, exhibiting a multi-peak pattern), and single day EEP (the entire EP occurs in only one day, with short duration and high intensity).

Among them, the unique balanced EEP includes two situations (Fig. 2). Firstly, precipitation lasts for an odd number of days and exceeds the 90th percentile in only one day, in addition to occurring in the middle of odd-numbered days. Secondly, precipitation lasts for an even number of days and only exceeds the 90th percentile in two days, thereby exhibiting symmetrical distribution on both sides. Considering feasibility, this study directly classified the first even-numbered unique balanced EEP as a balanced type, refined the second unique balanced EEP, compared EP observed in the two days, and reclassified and merged them into the front, late, or balanced EEP types. Therefore, in addition to single day EEP, all the other three EEP types included PSP.

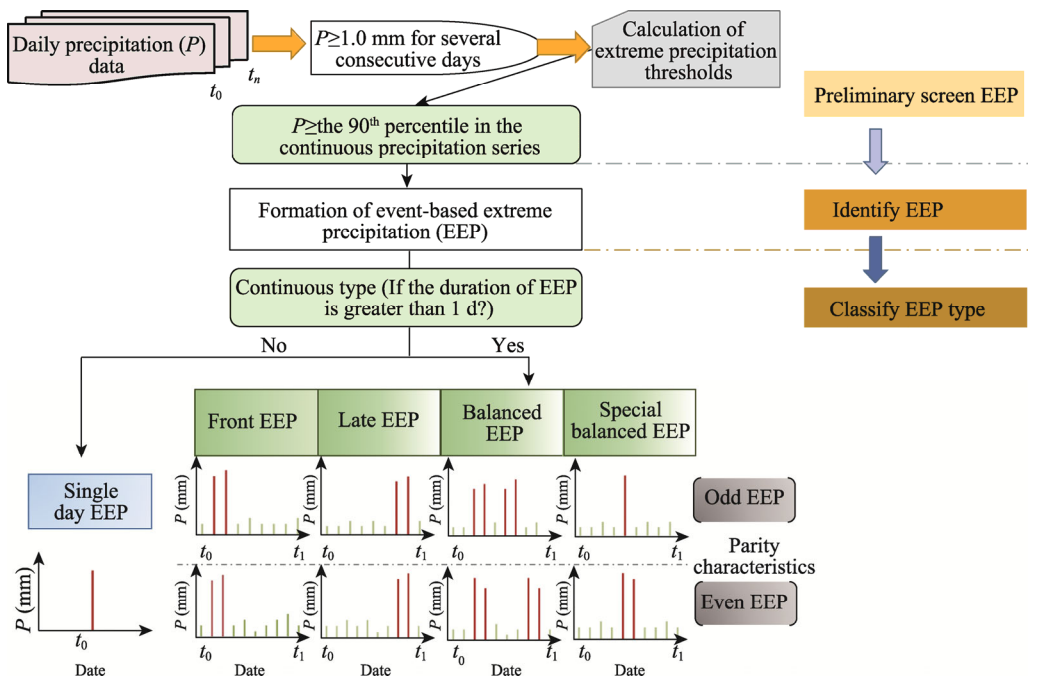

Fig. 2 Identification and classification of EEP types. t_0, t_1, and t_n represent the start date, end date, and any day of EEP, respectively. The red bars denote extreme precipitation (EP; P≥the 90th percentile in the continuous precipitation series) and the green bars represent non EP (P<the 90th percentile in the continuous precipitation series).

2.3.3 Data analysis methods

As a nonparametric method for trend estimation, the Theil-Sen estimator was used to analyze the trend of EP in different geomorphological zones on the LP. The modified Mann-Kendall (MMK) test was used to analyze the changing trend of EEP, and the accuracy of the trend calculation was improved by removing the influence of serial autocorrelation (Hamed and Rao, 1998). For the time series x_i=(x_1, x_2, …, x_n), the cross-correlation coefficient (S) was calculated as follows:

$$S = \sum_{i=1}^{n-1} \sum_{j=i+1}^{n} \mathrm{sgn}(x_j - x_i), \quad (1)$$

$$\mathrm{Var}^*(S) = \mathrm{Var}(S) \times \mathrm{Cor}, \quad (2)$$

$$\mathrm{Cor}=1+\frac{2}{n(n-1)(n-2)}\sum_{i=1}^{n-1}\rho_S(i)(n-1)(n-i-1)(n-i-2), \tag{3}$$

$$Z=\begin{cases}\dfrac{S-1}{\sqrt{\mathrm{Var}^*(S)}}, & S>0\\ 0, & S=0\\ \dfrac{S+1}{\sqrt{\mathrm{Var}^*(S)}}, & S<0\end{cases}, \tag{4}$$

where $\mathrm{sgn}(x_j-x_i)$ is a judgment function; i is the serial number of the starting value; j is the sequence number of the i+1st value; n is the sequence number of the last value; $\mathrm{Var}(S)$ is the variance of S; $\mathrm{Var}^*(S)$ is the modified variance of S; Cor represents the correction due to the autocorrelation of the time series; ρ_S is the sequence parameters; and Z is the standard normalization statistic. A positive value of Z indicates an increasing trend, while negative value signifies a decreasing trend.

Cross-wavelet analysis is a powerful method for studying multiscale and nonstationary signals in time series (Torrence and Compo, 1998; Grinsted et al., 2004). Assuming that $W_X(S)$ and $W_Y(S)$ are continuous wavelet transforms of sequences $X=\{x_1, x_2, \ldots, x_n\}$ and $Y=\{y_1, y_2, \ldots, y_n\}$, respectively, the equation of cross wavelet transform between them is:

$$W_n^{XY}(s)=W_n^X(s)W_n^{Y*}(s), \tag{5}$$

where $W_n^X(s)$ is the complete wavelet transform set of sequences X; $W_n^{Y*}(s)$ represents the complex conjugate of $W_n^Y(s)$; and $W_n^{XY}(s)$ is the cross wavelet power spectrum. It contains time, frequency, and amplitude information. The larger the value, the higher correlation between the two time series.

The Australian National University Spline (ANUSPLIN) spatial interpolation method, which was developed by an Australian scholar, Hutchinson, based on the thin plate smoothing spline theory, was employed in this study. A digital elevation model is introduced into the model as a variable or covariate for the interpolation of meteorological factors, which can reduce the systematic error caused by topographic factors associated with conventional interpolation methods (Hutchinson et al., 2009). According to the study, interpolation of meteorological data in complex terrain areas using ANUSPLIN is more accurate than other interpolation methods. The spatial resolution of this study is 30 m×30 m. A cross-validation method was used to test the

Table 2 Cross-validation results of spatial interpolation of precipitation

Type	Element	Signal	SNR	RMSE	RTVAR
Precipitation average	1960–1989	15.1	0.41	19.4000	35.1000
	1970–1999	12.0	0.37	13.5000	38.6000
	1980–2009	18.3	0.43	20.3000	50.5000
	1990–2019	14.9	0.38	24.6000	40.1000
	2000–2019	15.6	0.32	19.1000	46.4000
	2010–2019	17.2	0.37	19.9000	40.6000
Cumulative EEP frequency	Front EEP	10.9	0.23	0.0071	0.0155
	Late EEP	9.7	0.17	0.0068	0.0142
	Balanced EEP	11.4	0.21	0.0082	0.0193
	Single day EEP	9.5	0.19	0.0067	0.0167
Cumulative EEP volume	Front EEP	8.9	0.24	0.0072	0.0199
	Late EEP	11.3	0.18	0.0070	0.0224
	Balanced EEP	11.9	0.23	0.0056	0.0152
	Single day EEP	10.4	0.21	0.0091	0.0221

Note: EEP, event-based extreme precipitation; signal, the effective parameters or fitting spline degrees of freedom; SNR, signal-to-noise ratio; RMSE, root mean square error; RTVAR, the estimate of the standard deviation of the noise in the spline model.

accuracy of the interpolation results of the 14 precipitation elements (Table 2). The parameters evaluated included the effective parameters or fitting spline degrees of freedom (Signal), signal-to-noise ratio (SNR), root mean square error (RMSE), and the estimate of the standard deviation of the noise in the spline model (RTVAR), where an SNR value closer to 0.00 is considered a better interpolation effect. Similarly, a smaller RMSE value that is lower than the response time variability indicates relatively high interpolation accuracy. The 14 precipitation elements included in the interpolation results satisfied the accuracy requirements.

3 Results

3.1 Temporal and spatial variation characteristics of precipitation

3.1.1 Spatial patterns of precipitation changes

The ANUSPLIN-based spatial interpolation method was used to analyze the isoprecipitation belts during 1960–1989, 1970–1999, 1980–2009, 1990–2019, 2000–2019, and 2010–2019 (Fig. 3). Taking 30 a as the climatic period, the precipitation pattern on the LP was generally stable, and the multi-year average precipitation was 407.0 mm. Therefore, it can be concluded that the fluctuation direction of the 400.0 mm isoprecipitation belt (yellow and orange border) could indicate the basic variation characteristics of precipitation on the LP. Considering the 400.0 mm isoprecipitation belt as the boundary, the whole LP maintained a spatial pattern of "low in the northwest region and high in the southeast region". Notably, precipitation over the last 10 a (2010–2019) increased significantly when compared to precipitation during 1960–1989 (Table 3). The 500.0–600.0 mm isoprecipitation belt, which accounted for the largest proportion, has expanded by 51% to the

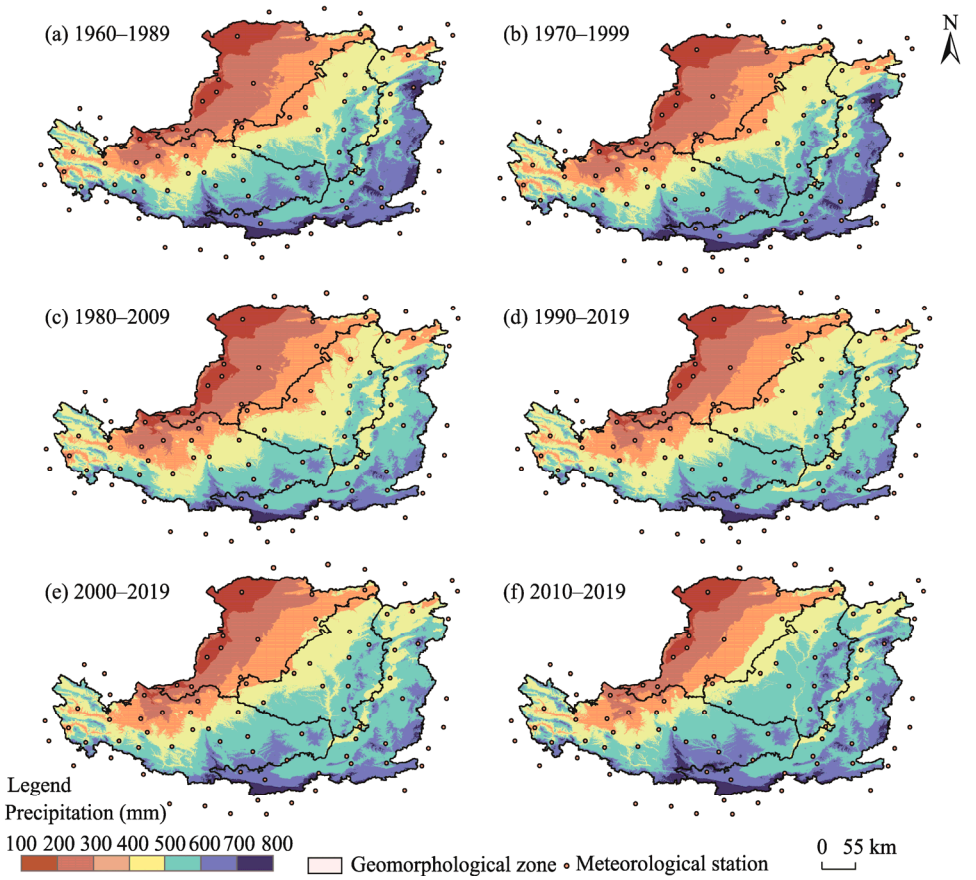

Fig. 3 Changes of the spatial patterns of precipitation during 1960–1989 (a), 1970–1999 (b), 1980–2009 (c), 1990–2019 (d), 2000–2019 (e), and 2010–2019 (f)

Table 3 Changes of typical isoprecipitation belts in the study area

PRCPTOT (mm)	1960–1989		1970–1999		1980–2009		1990–2019		2000–2019		2010–2019	
	Area ratio (%)	Change rate (%)	Area ratio (%)	Change rate between 1960–1989 and 1970–1999 (%)	Area ratio (%)	Change rate between 1970–1999 and 1980–2009 (%)	Area ratio (%)	Change rate between 1980–2009 and 1990–2019 (%)	Area ratio (%)	Change rate between 1990–2019 and 2000–2019 (%)	Area ratio (%)	Change rate between 1960–1989 and 2010–2019 (%)
≤200.0	5.31	-	5.08	–4.33	5.82	12.71	4.84	–16.84	4.61	–4.75	3.81	–28.25
200.0–300.0	13.53	-	14.30	5.69	13.81	–3.55	11.10	–19.62	11.09	–0.09	9.31	–31.19
300.0–400.0	14.27	-	16.05	12.47	16.59	3.25	16.46	–0.78	14.97	–9.05	12.21	–14.44
400.0–500.0	23.08	-	26.77	15.99	27.51	2.69	29.26	6.36	26.69	–8.78	20.51	–11.14
500.0–600.0	24.11	-	25.37	5.23	26.50	4.26	28.63	8.04	29.93	4.54	36.44	51.14
600.0–700.0	15.75	-	10.25	–34.92	8.12	–26.23	8.47	4.31	10.98	29.63	14.66	–6.92
≥700.0	3.95	-	2.18	–44.81	1.65	–32.12	1.24	–24.85	1.73	39.52	3.06	–22.53

Note: PRCPTOT represents the annual total wet-day precipitation and "-" denotes no data.

Table 4 Changes of typical EP belts in the study area

90pTOT (mm)	1960–1989		1970–1999		1980–2009		1990–2019		2000–2019		2010–2019	
	Area ratio (%)	Change rate (%)	Area ratio (%)	Change rate between 1960–1989 and 1970–1999 (%)	Area ratio (%)	Change rate between 1970–1999 and 1980–2009 (%)	Area ratio (%)	Change rate between 1980–2009 and 1990–2019 (%)	Area ratio (%)	Change rate between 1990–2019 and 2000–2019 (%)	Area ratio (%)	Change rate between 1960–1989 and 2010–2019 (%)
≤100.0	6.01	-	4.71	–21.63	5.43	15.29	3.85	–29.10	4.56	18.44	3.03	–49.58
100.0–200.0	35.09	-	33.10	–5.67	34.66	4.71	27.61	–20.34	30.25	9.56	20.34	–42.03
200.0–300.0	47.56	-	51.38	8.03	51.83	0.88	59.83	15.44	56.97	–4.78	49.12	3.28
300.0–400.0	10.80	-	10.31	–4.54	7.56	–26.67	8.24	8.99	7.67	–6.92	26.33	143.80
≥400.0	0.54	-	0.50	–7.41	0.52	4.00	0.47	–9.62	0.54	14.89	1.17	116.67

Note: 90pTOT represents total precipitation on very wet days and "-" denotes no data.

northwest region and mainly occurred in Zone II (Fig. 3d and f). The variations in the characteristics of EP were similar to those of annual precipitation. Over the last 10 a, the areas with EP≥300.0 mm increased significantly when compared to the previous periods (Table 4).

3.1.2 Temporal variation characteristics of EP

The overall response to EP in each zone of the LP was consistent. The results of correlation analysis between precipitation and EP in the four zones revealed that the correlation coefficient of precipitation was generally higher than that of EP, and the variables passed the significance test (P<0.05). The correlation of EP was stronger among different zones in the northwestern region (zones I, II, and III), the correlation coefficient was greater than 0.6, and the correlation coefficient with the southeastern region (Zone IV) was relatively low (<0.5). With regard to precipitation days, the overall correlation coefficient between annual precipitation days and EP days increased significantly. From the perspective of the overall response relationship between the zones, the northwestern regions (zones I and III) exhibited a strong consistency, while the junction regions (Zone II–Zone IV and Zone III–Zone IV) exhibited a certain transition. In addition, variations in the precipitation days among the four zones were consistent. Precipitation and precipitation days increased between 2010 and 2019. Using a 15-a moving average to retain the primary chronological trend, the variation trends of total precipitation and EP over the 60 a were generally insignificant (P>0.05; Fig. 4). An increasing trend in EP was observed over last 20 a, with that observed over the last 10 a passing the significance test (P<0.05). The recent significant increase observed in the trends of precipitation days and EP days could indicate a small fluctuation period embedded in a large time scale.

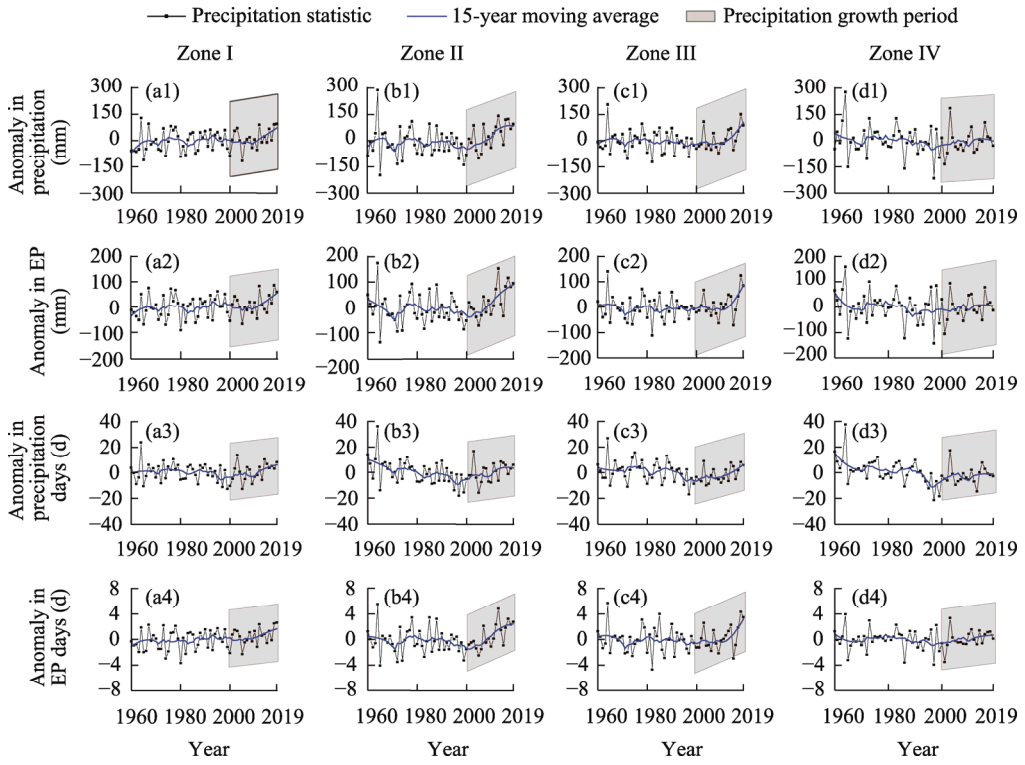

Fig. 4 Variations in precipitation and extreme precipitation (EP) in Zone I (a1–a4), Zone II (b1–b4), Zone III (c1–c4), and Zone IV (d1–d4) from 1960 to 2019

Trend analyses using typical EP indices can demonstrate the variations in EP more comprehensively (Table 5). The PRCPTOT, R12TOT, R50TOT, and 90pTOT indices characterizing precipitation exhibited an increasing trend in the western region of the LP (zones I, II, and III) and a decreasing trend in the eastern region of the LP (Zone IV; $P>0.05$). Furthermore, R12TOT was a key empirical indicator of precipitation and ecology on the LP. R12TOT exhibited an increasing trend in the central and western region of the LP (zones I, II, and III) throughout the study period. R50TOT was mainly associated with Zone IV, and the proportion of heavy precipitation (>100.0 mm) increased from the northwest to the southeast regions with the R50TOT. The marginal stations located in the southeastern region (Zone IV) experienced up to 30% of the R50TOT. Pday and FSPday exhibited a downward trend during the entire study period, while the corresponding SDII increased significantly ($P<0.05$). Based on the relationship between Pday and SDII, we can see that precipitation intensity in Zone II was closely associated with the variation in annual precipitation, whereas the precipitation intensity in Zone III was closely associated with precipitation occurring in flood season.

Table 5 Inter-annual variation trends of EP indices from 1960 to 2019

Index	Zone I		Zone II		Zone III		Zone IV		Total area	
	Slope#	Mean	Slope#	Mean	Slope#	Mean	Slope#	Mean	Slope#	Mean
PRCPTOT (mm)	0.60	246.00	1.08	438.50	0.42	409.20	–0.26	536.10	0.38	407.50
R12TOT (mm)	0.48	127.10	0.98	255.60	0.42	204.20	–0.09	343.20	0.42	232.50
R50TOT (mm)	0.01	18.40	0.17	38.80	0.16*	19.60	–0.38*	72.30	–0.01	37.30
90pTOT (mm)	0.37	127.30	0.52	216.20	0.33	196.60	–0.22	277.70	0.33	204.40
Pday (d)	–0.04	54.20	–0.12*	78.20	–0.15	90.10	–0.25*	83.60	–0.15*	76.50
FSPday (d)	–0.01	32.60	–0.06	42.40	–0.10*	47.20	–0.12*	42.50	–0.08*	41.20
SDII (mm/d)	0.01*	4.40	0.02*	5.60	0.01*	4.50	0.02*	6.40	0.01*	5.22

Note: # represents that the slope is dimensionless and * indicates significant trend ($P<0.05$).

3.2 Variations in EEP types

According to the results of the previous section, SDII exhibited a significant trend during the entire period and across the region; that is, the number of precipitation days decreased when total precipitation did not vary considerably, resulting in a significant increase in the precipitation intensity. The phenomenon could imply that the types of annual precipitation (intra-annual form of systematic and continuous precipitation as well as sudden precipitation) varied to a certain extent. If annual precipitation is represented on a relatively small-scale (event scale), the significant trend exhibited by SDII may reflect variations in the peaks and locations of events. Therefore, it is necessary to further illustrate EP at the event scale.

3.2.1 Intra-annual characteristics of EEP

Statistical analyses of the frequency characteristics of EEP in each month from 1960 to 2019 showed that the four EEP types mainly occurred from May to September, accounting for more than 85% of the total annual EEP types (Fig. 5). The annual peak for single day EEP occurred in August, while those of the other three EEP types (front, late, and balanced EEP types) occurred in July. The kurtosis of single day EEP was high, that is, the distribution was more concentrated during the year, while the kurtosis of late EEP was relatively low. Very few EEP types have occurred from December to February.

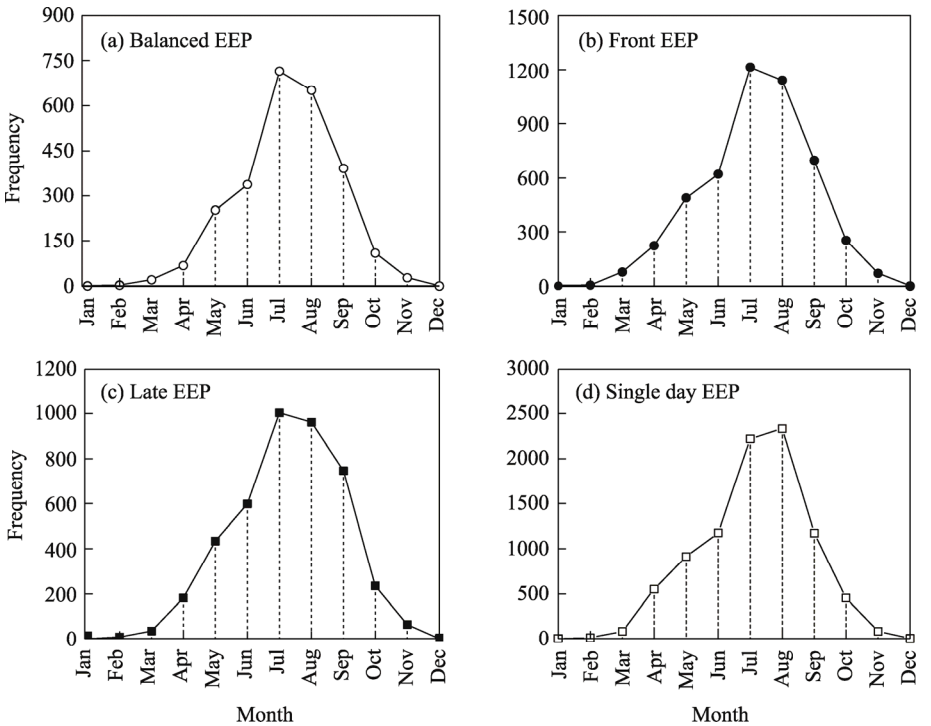

Fig. 5 Characteristics of the intra-annual change of balanced EEP (a), front EEP (b), late EEP (c), and single day EEP (d) from 1960 to 2019

3.2.2 Dominant types of EPP

A comparison of cumulative precipitation and cumulative frequencies revealed that the spatial distribution of EEP types on the LP was complex (Figs. 6 and 7). Cumulative precipitation and frequencies in the entire region varied; however, the overall trend of the dominant type of EEP was consistent (Figs. 6–8). First, the cumulative frequency of single day EEP on the whole LP was 43%, that of front EEP was slightly higher than 23%, that of late EEP was approximately 21%, and that of balanced EEP was the lowest, with a multi-year average of 13%. Therefore, based on the cumulative frequency, we concluded that the LP is dominated by single day EEP. In

addition, the cumulative precipitation of single day EEP was much higher than those of the other three EEP types, with an average value of 34%. Notably, the cumulative precipitation of balanced EEP, which had the lowest frequency, was not significantly different from those of front and late EEP types, which did not exhibit the characteristics of low frequency that corresponded to low precipitation, and its cumulative precipitation percentage was higher than 20%. Based on spatial clustering of the zones, the cumulative frequencies of EEP and precipitation were inconsistent with response in some areas. Single day EEP was mainly distributed in Zone I, which is a typical positive response region with high cumulative frequency and high precipitation. Zones II and III exhibited the same positive response, while the southern region of Zone IV exhibited a negative response. From the perspective of spatial dispersion (Fig. 8), the standard deviation (SD) values of the cumulative frequencies of single day and late EEP types were relatively high. The SD values of the accumulated precipitation of EEP for single day and balanced EEP types were relatively high. However, the SD values were less than 0.08, indicating that the internal spatial heterogeneity of the four EEP types in the various zones was only a relative state and the spatial variations among the four EEP types remain dominant across the LP.

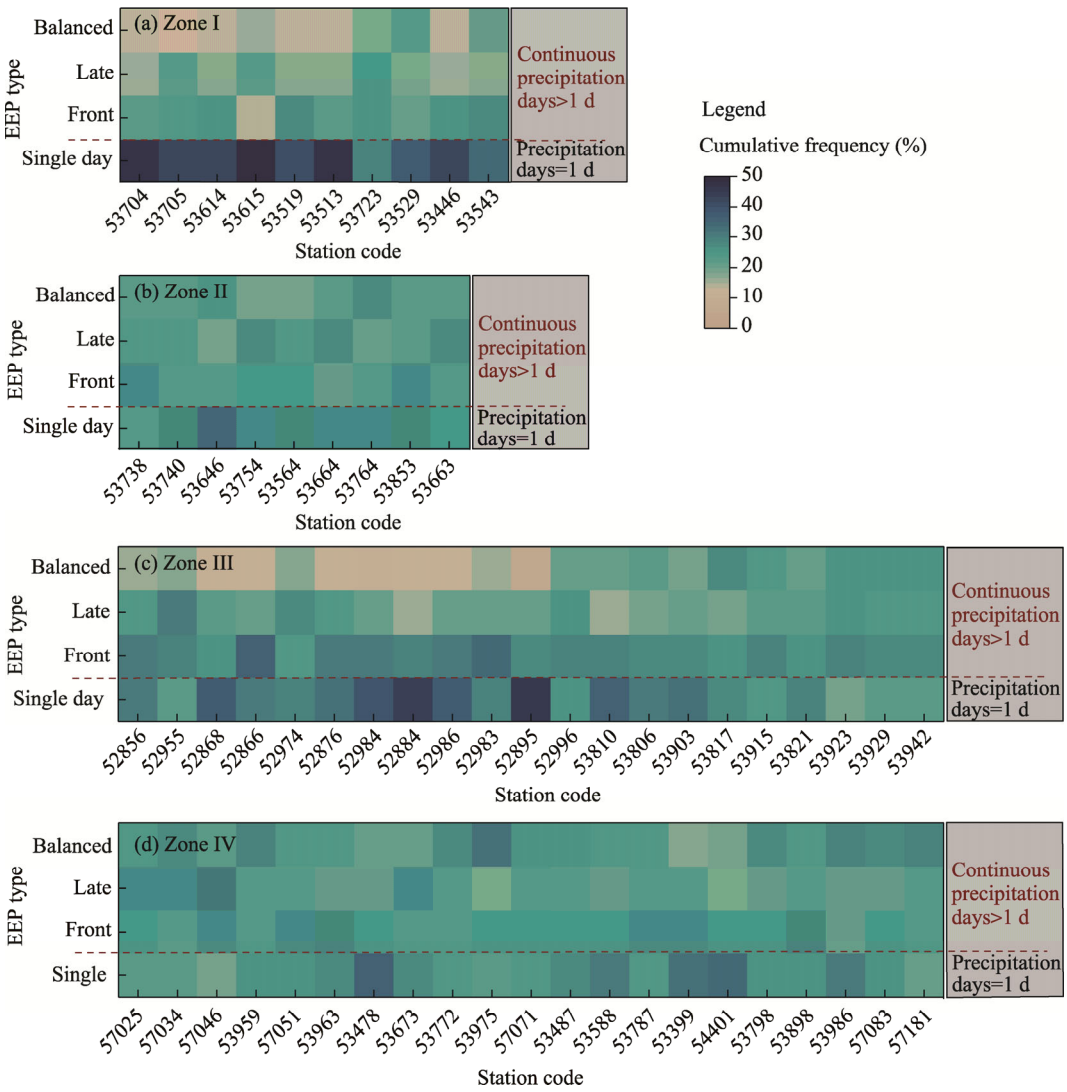

Fig. 6 Cumulative frequency of the four EEP types in Zone I (a), Zone II (b), Zone III (c), and Zone IV (d)

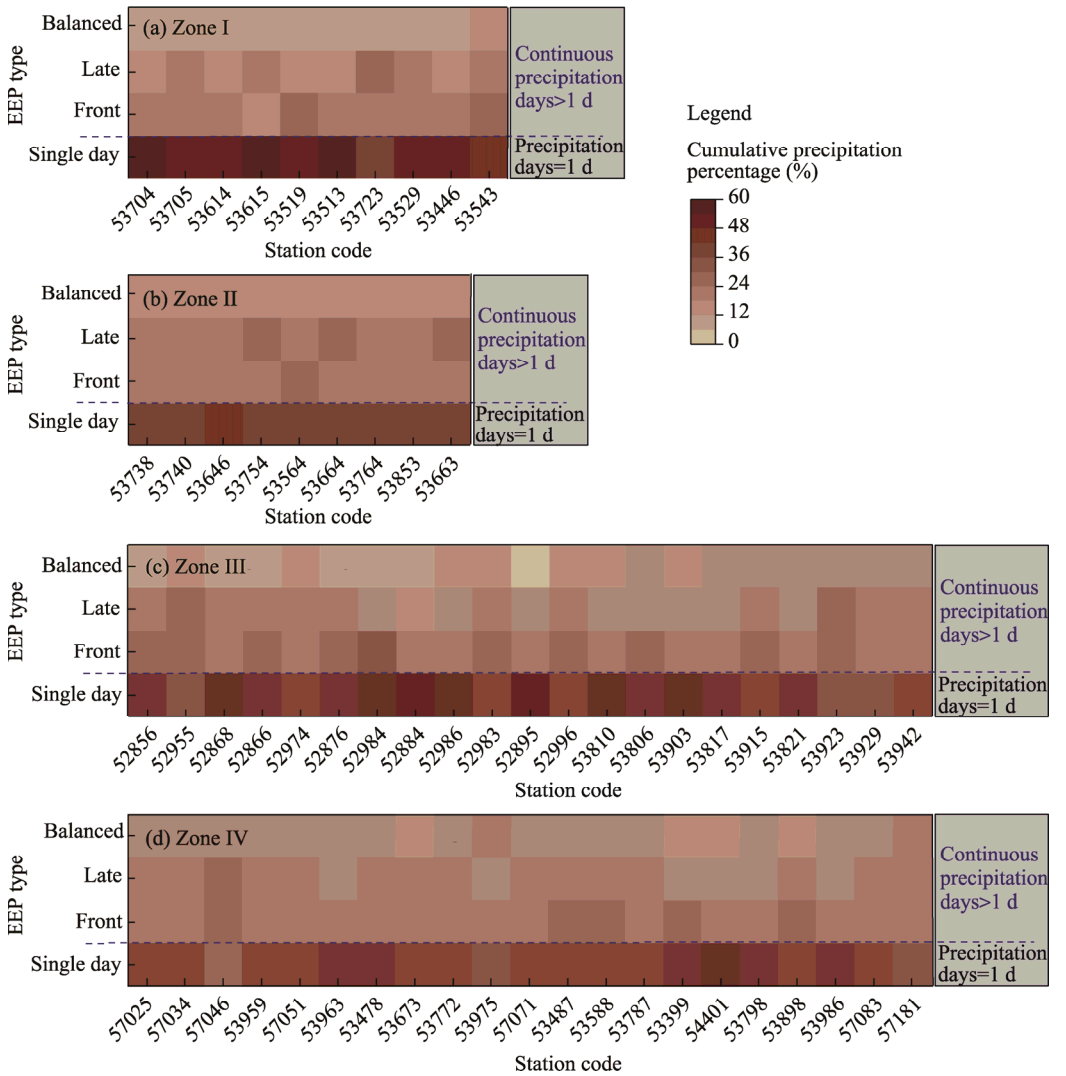

Fig. 7 Cumulative precipitation percentage of the four EEP types in Zone I (a), Zone II (b), Zone III (c), and Zone IV (d)

3.2.3 Variation trends of EEP types

The cumulative precipitation distribution of the four EEP types across the various zones varied over the four time periods (Fig. 9). The predominant single day EEP exhibited a gradual increase in the cumulative precipitation percentage, and the change was consistent throughout the whole LP. The precipitation percentage of late EEP exhibited an increasing trend in the western region (zones I, II, and III). The precipitation percentage of balanced EEP increased significantly in the southeastern region (Zone IV). The precipitation percentages of various events in each zone were slightly different, and the coefficient of variation was less than 0.08, with the major variations being reflected in the EEP types.

With regard to the trend analysis for the four EEP types at each station from 1960 to 2019 (Fig. 10), the variation trends of the various EEP types on the LP increased, and the trends identified could be divided into two categories. The first category comprised stations that exhibited significant increases in EEP, with the most dominant type being single day EEP, which was distributed across the whole region (P<0.05). The second category comprised stations that exhibited fluctuations in EEP (P>0.05), and most stations across the region belonged to the second category. The increasing trend in EEP was mainly observed in western region of the LP

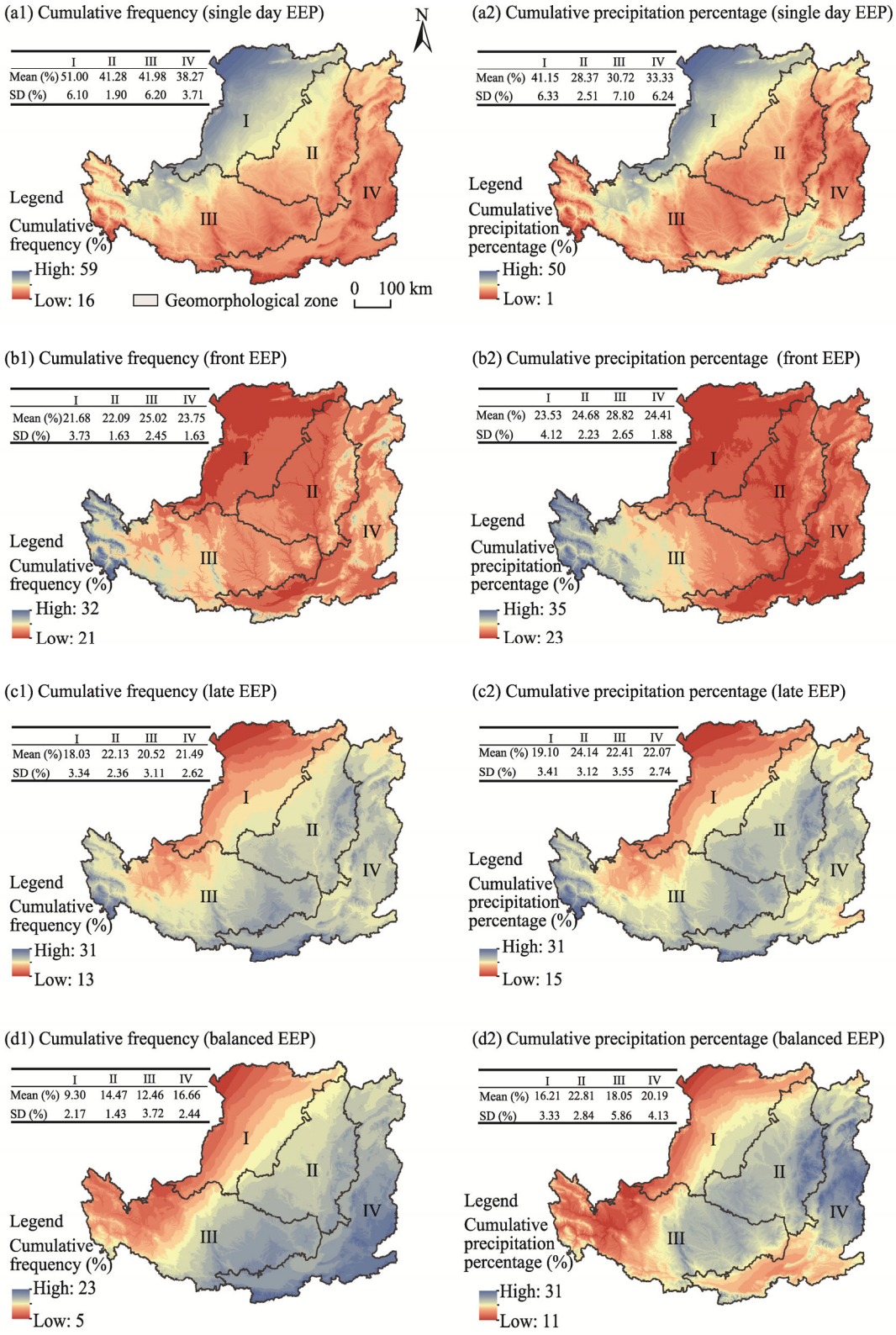

Fig. 8 Spatial distribution of cumulative frequency and cumulative precipitation percentage of single day EEP (a1 and a2, respectively), front EEP (b1 and b2, respectively), late EEP (c1 and c2, respectively), and balanced EEP (d1 and d2, respectively)

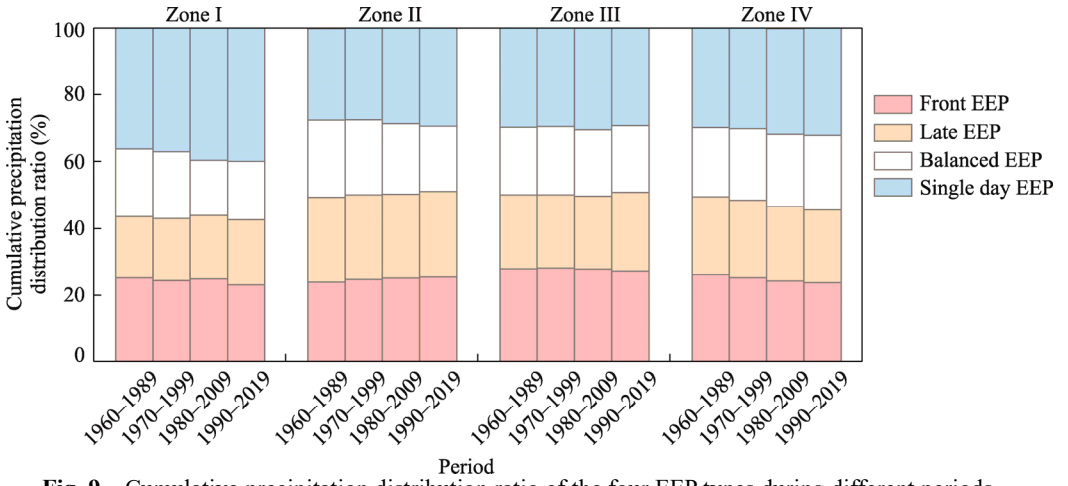

Fig. 9 Cumulative precipitation distribution ratio of the four EEP types during different periods

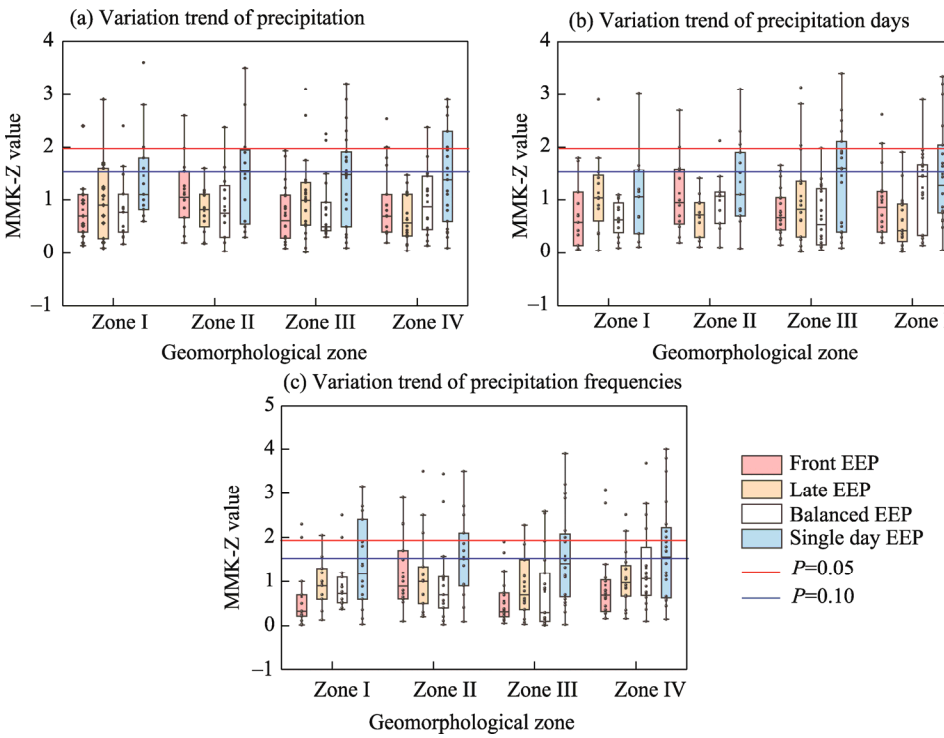

Fig. 10 Variation trend of precipitation (a), precipitation days (b), and precipitation frequencies (c) of the four EEP types. MMK-Z value is the standard normalization statistic in the modified Mann-Kendall (MMK) test. The box represents the significant characteristics of precipitation trends for the four EEP types at stations in different zones. The short border of the boxes represents the range from the lower quantile (Q25) to the upper quantile (Q75). The dots and horizontal lines inside the boxes represent the means and medians, respectively. The dots outside the boxes represent outliers. The upper and lower whiskers indicate the maximum and minimum values, respectively.

(zones I, II, and III). EEP at most stations in the southeastern region of the LP (Zone IV) exhibited a decreasing trend, except for single day EEP. Therefore, the EEP of some stations did not change significantly in the long run, and the increasing or decreasing trend was a temporal fluctuation, which requires further study.

3.2.4 Contribution of EP to EEP

Over the last 60 a, the precipitation proportion caused by single day EEP, which was the dominant

EEP type on the LP, accounts for 43% of the total EEP (Figs. 7 and 8). However, the remaining three EEP types accounted for more than 50% of the total EEP over the 60 a. The EEP value obtained in this study was theoretically greater than the sum of the precipitation corresponding to EP days. Therefore, the difference between EEP and EP reflected PSP level in the EEP, or the contribution of precipitation to the event on EP days. Here, the *C* value is used to represent the contribution of EP to EEP, the formula is as follows:

$$C \text{ value}=\text{EP}/\text{EEP}. \quad (6)$$

When EEP is a single day EEP type, *C* value=1; when EEP is the other three EEP types, *C* value <1. The smaller the *C* value, the greater the contribution of PSP in EEP.

The *C* values for all stations on the LP from 1960 to 2019 were in the range of 0.67–0.83, indicating a cumulative PSP ratio of 0.17–0.33 (Fig. 11). Spatially, *C* value increased gradually from the northwest region to the southeast region with an increase in the average precipitation. The PSP of some stations in the eastern region (Zone IV) reached a third of the EEP, which could be associated with the amount of annual precipitation and number of precipitation days in the southeastern region of the LP. Furthermore, some stations in Zone IV received precipitation of more than 650.0 mm, and the number of annual precipitation days were more than 150 d, which could lead to an increased probability of continuous precipitation with high PSP.

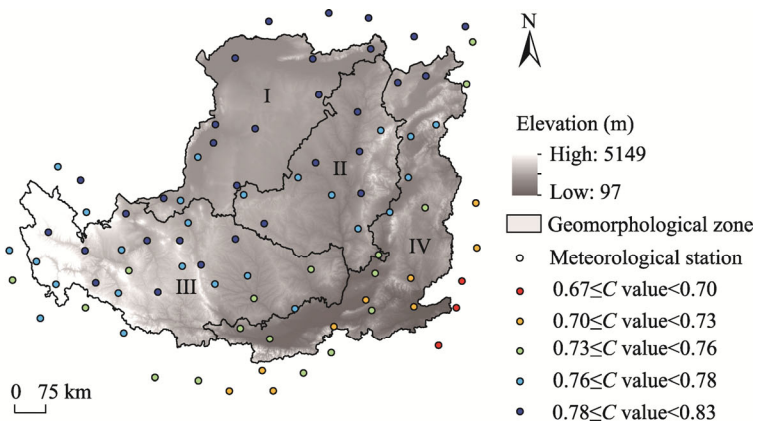

Fig. 11 Spatial distribution of the *C* value. *C* value represents the contribution of EP to EEP.

4 Discussion

4.1 Rationality of EEP concept application on the Loess Plateau (LP)

The distribution characteristics of *C* values from the northwest region to the southeast region on the LP indicate that the manifestation of PSP in EEP is more pronounced in the areas with persistent and high levels of precipitation. The EP and PSP are superimposed together to form a regional rainstorm-runoff, which is an objective part of the runoff process. The method applied in this study is based on the persistent characteristics of precipitation and does not separate EP from the precipitation process. Therefore, the method could be reliable for the analysis of flood disasters in river basins that receive continuous and high amounts of precipitation, such as the middle and lower reaches of the Yangtze River of China, northeastern India, and the Amazon basin in South America (Lin et al., 2020).

The dominant type of continuous EEP at local stations should be taken into consideration. The definition of the precipitation peak position for EP in this study is similar to the precipitation peak parameter in a hydrological model. A few studies have shown that the precipitation pattern following the rain peak has greater pressure on the outlet of the pipe network or the downstream reservoir (Dunkerley, 2012). Moreover, the regional rainstorm disasters exert a certain hysteresis effect and may exacerbate flooding (Liu et al., 2009; Luo and Chen, 2015). Consequently, it is a sensitive parameter of the hydrological model. For example, Suide Hydrological Station (No.

53754) is one of the stations that has experienced frequent summer rainstorms and floods on the LP over the last 30 a. The area where Suide Hydrological Station is located is dominated by single day EEP, but the station has the highest frequency of late EEP (Figs. 6 and 7). Therefore, high incidences of the short-term single day EEP and continuous late EEP, in addition to the poor surface environment in the local area, could become a disaster risk. However, further studies should be conducted using more local flood disaster data.

4.2 The LP may be the transition area for EEP characteristics

According to the frequency and temporal distribution data of EEP on the LP (Figs. 6 and 8), continuous EEP observed in the region lying to the west of Zone III was relatively high, which could indicate a transition of the EEP features from the LP to the Tibetan Plateau (the first step of China's topography). Furthermore, the balanced EEP was dominant in the southeastern region of Zone IV, which reduces the frequency difference among the four EEP types, suggesting the transition of EEP features from the LP to the Qinling Mountains and the Yangtze River Basin (the third step of China's topography) (Li et al., 2020). A few studies have revealed that the prediction results of EP in high latitude and high altitude areas, as well as other plains vary considerably in temporal distributions based on multiple climate datasets (Xu et al., 2019). Therefore, we speculate that the LP is not only a transition area for topography and climate in China, but also a transition area for EEP characteristics, which requires verification using data from several typical watersheds.

4.3 Responses of EEP types to regional warming

Despite the recent global warming stagnation, the LP experienced accelerated warming between 1990 and 2010 (Sun et al., 2015). The temperature variation on the LP exhibits both temporal and spatial differences. The spatial distribution of the increase in temperatures on the LP is uneven, and the growth rate of temperature in the northwestern region of the LP (Zone I) is significantly higher (up to 0.41°C/10 a) than those in the other three zones; the rate is almost twice that of the slowest warming zone (Zone IV) (Liu, et al., 2021). Therefore, the two angles of linear correlation and multiple wavelet coherence were selected to analyze the relationship between EEP types and temperature on the LP.

According to the results of linear correlation analyses, the four EEP types on the LP exhibited a marked response to the overall regional warming (Table 6). The index of single day EEP exhibited a significant positive correlation with temperature and no significant positive correlations were observed between late and balanced EEP types and temperature in most regions. The indices of the four EEP types were almost positively correlated with temperature in the northwestern region of the LP (zones I, II, and III), with a partial negative correlation being observed in the southeastern region (Zone IV). The results are consistent with the research trend of increasing short-duration heavy precipitation in the mid-latitudes under global warming conditions. In addition, the results verify the spatial pattern of changes in the average EP belt on the LP shifting gradually to the northwestern region, which is an area with low annual average precipitation but increased EP (Table 5).

The nonlinear and multi-scale wavelet coherence results of EEP and temperature for the various zones revealed the following (Fig. 12). First, EEP in the western region of the LP (zones I, II, and III) was almost positively correlated with temperature; that is, EEP increased with an increase in warming, while EPP in Zone IV decreased with an increase in temperature, except for the single day EEP. Second, the relationship between EEP and temperature exhibited periodicity and had stages. For example, the balanced EEP in Zone IV exhibited a negative correlation with temperature over the 1960–1970 period, which was a short period (3–7 a), and then the correlation gradually decreased. After 1990, the negative correlation observed between the balanced EEP and temperature in the region increased gradually, with the main period transitioning from a short period during the early stage to medium and long periods (6–10 a). The observation could be attributed to the variation in warming rates across different periods, with

temperature increases in the subregions differing substantially after 1990. For example, the rate of increase in average temperature in Zone I from 1960 to 1989 was gradual and fluctuated (0.23°C/10 a; R^2=0.14), whereas the rate of temperature increase from 1990 to 2019 was steady (0.31°C/10 a; R^2=0.26). Third, the correlation between single day EEP and temperature shifted periodically over time, and a strong correlation was observed almost throughout the study period. Moreover, relatively long periods were observed in zones II and IV, suggesting that the relationship between single day EEP and warming in the two zones was relatively stable during the interdecadal period.

Table 6 Correlations between EEP types and temperature on the Loess Plateau

EEP type	Index	Zone I		Zone II		Zone III		Zone IV	
		Correlation coefficient	Sig	Correlation coefficient	Sig	Correlation coefficient	Sig	Correlation coefficient	Sig
Front EEP	Precipitation	–0.15	0.57	0.27*	0.98	0.44	0.77	–0.23	0.59
	Day	–0.21	0.71	0.10	0.45	0.38	0.63	–0.29	0.43
	Frequency	–0.15	0.81	0.10*	0.95	0.41	0.34	–0.25	0.82
Late EEP	Precipitation	0.25*	0.99	0.25	0.46	0.25*	1.00	–0.34	0.76
	Day	0.35*	0.98	0.43	0.35	0.36	0.67	–0.46	0.35
	Frequency	0.18	0.54	0.20	0.79	0.17	0.56	–0.09	0.75
Balanced EEP	Precipitation	0.11	0.43	0.23	0.58	0.18	0.83	–0.27*	0.98
	Day	0.31	0.33	0.13	0.49	0.26	0.38	–0.36*	0.97
	Frequency	0.08	0.50	0.19	0.42	0.13	0.72	–0.20	0.65
Single day EEP	Precipitation	0.44*	1.00	0.49*	1.00	0.40*	1.00	0.51*	1.00
	Day	0.49*	0.99	0.42*	0.99	0.38*	1.00	0.49*	1.00
	Frequency	0.31*	0.99	0.41*	0.99	0.38*	1.00	0.44*	0.99

Note: Sig is significance value. * represents the significant correlations between EEP and temperature at P<0.05 level.

In addition to the influence of uneven regional warming, the spatial variations in precipitation factors on the LP are closely associated with the locations of weather systems, such as the subtropical region and the Qinghai–Tibet Plateau. The western El Niño region can also be regarded as a key region corresponding to EP on the LP (Li et al., 2022; Lu et al., 2022). The EEP, PRCPTOT, and R12TOT in the northwest region of LP showed an insignificant increasing trend, which may be attributed to the changes in evapotranspiration in the local area. Since 1980, the vegetation restoration rate has increased significantly with the vigorous implementation of ecological projects in the northwest region of the LP, and the enhanced transpiration from vegetation could affect the water circulation process in the watershed, which may further increase EP in local areas (Feng et al., 2016; Zhang et al., 2020). Wang (2006) revealed that the western part of the LP exhibits the characteristics of humidification, whereas the eastern part experiences aridification in summer, and that summer precipitation on the LP is dominated by EP. The EP days only account for 13% of the total summer precipitation days, while it accounts for approximately 54% of the total precipitation. The proportion of EP in the total summer precipitation in 70% of the stations has been on the rise, and the FSPday index has decreased significantly, which indicates that summer precipitation in the form of EEP on the LP is likely to become more frequent (Wang et al., 2006; Lu et al., 2022). Overall, EEP on the LP is closely associated with temperature changes, especially the overall variation in the correlation between the western and southeastern regions. The increase in EEP in the northwestern region of the LP indicates, to a certain extent, the potential increase in water resources in the arid region of northwestern China (Han et al., 2020), which may be a favorable indicator owing to the current water scarcity situation in the arid regions of northwestern China. However, the effective precipitation caused by PSP and the increase in continuous EEP are more likely to exacerbate local flood disasters.

Furthermore, short-duration precipitation and high-intensity single day EEP could continue to increase in the future with the increase in regional warming rates, which may aggravate soil erosion and result in certain ecological risks in zones II and III that are characterized by high soil erodibility (Cui et al., 2020; Jia et al., 2021). Regional variations in EP are influenced by several other factors, especially topography and urbanization, and therefore require further studies (Paul et al., 2018; Wu et al., 2021).

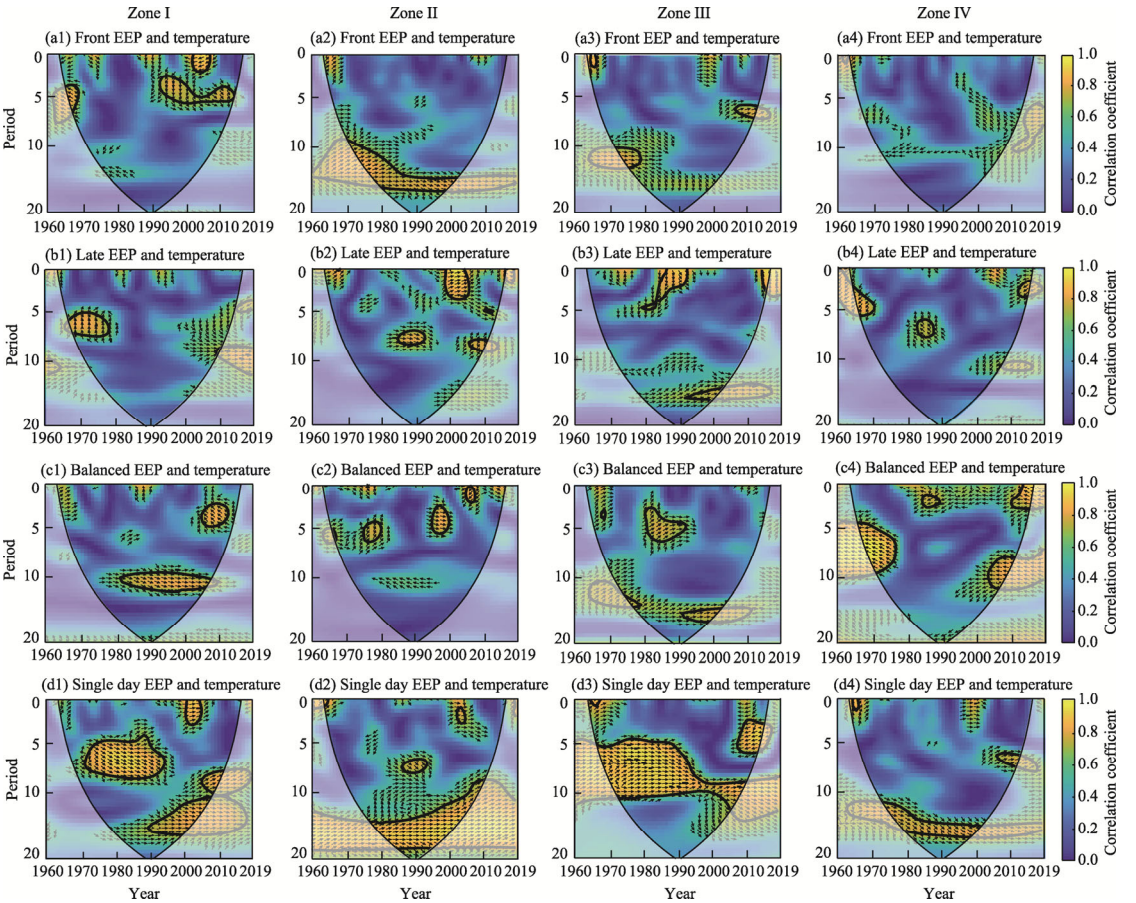

Fig. 12 Wavelet coherence analysis of the four EEP types and temperature in Zone I (a1–a4), Zone II (b1–b4), Zone III (c1–c4), and Zone IV (d1–d4). The thick black contour designates the correlations beyond the 95% significance level against the red noise. The cone of influence where edge effects might distort the picture is shown as a lighter shade. The relative phase relationship is indicated by the arrow direction, with in-phase pointing right and anti-phase pointing left. The color bar on the right denotes correlation coefficient, with 0.0 representing no correlation and 1.0 indicating strong relationship.

5 Conclusions

In this study, we used EP indices to elucidate the overall temporal and spatial variation characteristics of EP on the LP based on the daily precipitation data obtained from 87 meteorological stations on the LP from 1960 to 2019. Similarly, we also classified the EP events into four EEP types based on the precipitation time scales, and analyzed the temporal and spatial distribution patterns of the four EEP types. In addition, the relationship between EP and regional warming was determined. The results showed that the precipitation on the LP generally maintains a spatial pattern of "low in the northwest region and high in the southeast region". The 400.0 mm precipitation belt has gradually shifted to the northwest region. Precipitation has increased significantly over the last 10 a. PRCPTOT, 90pTOT, and R12TOT exhibited an increasing trend in

the western region (zones I, II, and III), but showed a decreasing trend in the eastern region (Zone IV) of the LP. SDII exhibited a significant increasing trend across the LP. The cumulative precipitation and frequency of single day EEP were the highest, while those for balanced EEP were the lowest on the LP over the 60 a. EEP is closely associated with regional warming. Continuous EEP increased in the northwestern region (zones I, II, and III) but tended to decrease in the eastern region (Zone IV) following an increase in temperatures. Single day EEP is likely to increase with an increase in temperature across the LP in the future.

Acknowledgements

This research was supported by the National Natural Science Foundation of China (52022081), and the Technology Project Funded by Clean Energy and Ecological Water Conservancy Engineering Research Center of China (QNZX-2019-03).

References

Aihaiti A, Jiang Z H, Zhu L H, et al. 2021. Risk changes of compound temperature and precipitation extremes in China under 1.5°C and 2°C global warming. Atmospheric Research, 264: 105838, doi: 10.1016/j.atmosres.2021.105838.

Back A J. 2011.Time distribution of heavy rainfall events in Urussanga, Santa Catarina State, Brazil. Acta Scientiarum Agronomy, 33(4): 583–588.

Caballero W, Rahman A. 2013. Variability in rainfall temporal patterns: a case study for New South Wales, Australia. Journal of Hydrology and Environment Research, 1(1): 41–48.

Cui Y S, Pan C Z, Liu C L, et al. 2020. Spatiotemporal variation and tendency analysis on rainfall erosivity in the Loess Plateau of China. Hydrology Research, 51(5): 1048–1062.

Ding Y H, Liang P, Liu Y J, et al. 2020. Multiscale variability of Meiyu and its prediction: A new review. Journal of Geophysical Research: Atmospheres, 125(7): e2019JD031496, doi: 10.1029/2019JD031496.

Donat M G, Lowry A L, Alexander L V, et al. 2016. More extreme precipitation in the world's dry and wet regions. Nature Climate Change, 6: 508–513.

Donat M G, Angélil O, Ukkola A M. 2019. Intensification of precipitation extremes in the world's humid and water–limited regions. Environmental Research Letters, 14(6): 065003, doi: 10.1088/1748-9326/ab1c8e.

Dunkerley D. 2012. Effects of rainfall intensity fluctuations on infiltration and runoff: rainfall simulation on dryland soils, Fowlers Gap, Australia. Hydrological Process, 26(15): 2211–2224.

Feng X, Fu B, Piao S, et al. 2016. Revegetation in China's Loess Plateau is approaching sustainable water resource limits. Nature Climate Change, 6: 1019–1022.

Fu S H, Yang Y F, Liu B Y, et al. 2020. Peak flow rate response to vegetation and terraces under extreme rainstorms. Agriculture, Ecosystems & Environment, 288: 106714, doi: 10.1016/j.agee.2019.106714.

Gao H D, Li Z B, Li P, et al. 2018. Paths and prevention and control of heavy rain and sediment production in the Loess Plateau-based on the understanding of the 2017-07-26 heavy rain in the Wuding river basin. China Soil and Water Conservation Science, 16(4): 66–72. (in Chinese)

Gao Y, Feng Q, Liu W, et al. 2015. Changes of daily climate extremes in Loess Plateau during 1960–2013. Quaternary International, 371: 5–21.

Ghassabi Z, Kamali G A, Meshkatee A H, et al. 2016. Time distribution of heavy rainfall events in south west of Iran. Journal of Atmospheric and Solar-Terrestrial Physics, 145: 53–60.

Grinsted A, Moore J C, Jevrejeva S. 2004. Application of the cross wavelet transform and wavelet coherence to geophysical time series. Nonlin Processes Geophys, 11: 561–566.

Guo E L, Zhang J Q, Wang Y F, et al. 2019. Spatiotemporal variations of extreme climate events in Northeast China during 1960–2014. Ecological Indicators, 96: 669–683.

Guo M M, Yang B, Wang W L, et al. 2019. Distribution, morphology and influencing factors of rills under extreme rainfall conditions in main land uses on the Loess Plateau of China. Geomorphology, 345: 106847, doi: 10.1016/j.geomorph.2019.106847.

Hamed K H, Rao A R. 1998. A modified Mann-Kendall trend test for autocorrelated data. Journal of Hydrology, 204(1–4): 182–196.

Hamidreza M G, Hasan A, Mohammad J, et al. 2010. Study of the temporal distribution pattern of rainfall effect on runoff and sediment generation using rain simulator. World Applied Sciences Journal, 11: 64–69.

Han X Q, Zhao Y, Gao X R, et al. 2020. Virtual water output intensifies the water scarcity in Northwest China: Current situation, problem analysis and countermeasures. Science of the Total Environment, 765(11): 144276, doi: 10.1016/j.scitotenv.2020.144276.

Hitchens N M, Brooks H E, Schumacher R S. 2013. Spatial and temporal characteristics of heavy hourly rainfall in the United States. Monthly Weather Review, 141(12): 4564–4575.

Hu L, Li Y D, Song Y, et al. 2011. Seasonal variability in tropical and subtropical convective and stratiform precipitation of the East Asian monsoon. Science China Earth Sciences, 54(10): 1595–1603.

Hutchinson M F, Mckenney D W, Lawrence K, et al. 2009. Development and testing of Canada-wide interpolated spatial models of daily minimum-maximum temperature and precipitation for 1961–2003. Journal of Applied Meteorology & Climatology, 48(4): 725–741.

IPCC. 2014. Climate Change 2014: Synthesis Report: Contribution of Working Groups I, II and III to the Fifth Assessment Report of the Intergovernmental Panel on Climate Change. [2022-01-10]. https://www.ipcc.ch/report/ar5/syr/.

IPCC. 2021. Climate Change 2021: The Physical Science Basis. Contribution of Working Group I to the Sixth Assessment Report of the Intergovernmental Panel on Climate Change. [2022-02-15]. https://www.ipcc.ch/report/ar6/wg1/.

Jia L, Yu K X, Li Z B, et al. 2021. Temporal and spatial variation of rainfall erosivity in the Loess Plateau of China and its impact on sediment load. CATENA, 210: 105931, doi: 10.1016/j.catena.2021.105931.

Jin F M, Yang W C, Fu J X, et al. 2021. Effects of vegetation and climate on the changes of soil erosion in the Loess Plateau of China. Science of the Total Environment, 773: 145514, doi: 10.1016/j.scitotenv.2021.145514.

Jin S Y, Gao W Y, Luo S W, et al. 2018. Analysis on the return period of "7.26" rainstorm and flood in 2017 in the Wudinghe basin. MATEC Web of Conferences, 246: 01105, doi: 10.1051/matecconf/201824601105.

Li J J, Feng Z D, Tang L Y. 1988. Late quaternary monsoon patterns on the Loess Plateau of China. Earth Surface Processes and Landforms, 13(2): 125–135.

Li S S, Wang C B, Yan J P, et al. 2020. The temporal and spatial variation characteristics of extreme precipitation in the north and south of the Qinling mountains oriented to the event process. Acta Geologica Sinica, 75: 989–1007. (in Chinese)

Li S S, Kong F, Han L, et al. 2022. The temporal and spatial variation characteristics of extreme precipitation in the Loess Plateau of northern Shaanxi and its influencing factors. Geographical Research, 39(1): 140–151. (in Chinese)

Liu L Y, Lu R J, Ding Z Y, et al. 2021. Analysis on the characteristics and causes of climate change in the Loess Plateau. Journal of the Earth Environment, 12: 615–631. (in Chinese)

Lin Q G, Wang Y, Glade T, et al. 2020. Assessing the spatiotemporal impact of climate change on event rainfall characteristics influencing landslide occurrences based on multiple GCM projections in China. Climatic Change, 162: 761–779.

Liu S Y, Huang S Z, Xie Y Y, et al. 2018. Spatial-temporal changes of rainfall erosivity in the Loess Plateau, China: changing patterns, causes and implications. CATENA, 166: 279–289.

Liu Y H, Tang C, Li T F, et al. 2009. Study on the relationship between geological hazards and rainfall patterns. Journal of Engineering Geology, 17: 6–10. (in Chinese)

Liu Z H, Wu G C. 2021. Quantifying the precipitation-temperature relationship in China during 1961–2018. International Journal of Climatology, 42(5): 2656–2669.

Lu S, Hu Z Y, Fu C W, et al. 2022. Analysis of extreme precipitation in the Loess Plateau in summer and its causes. Plateau Meteorology, 41(1): 241–254. (in Chinese)

Luo Y, Chen Y. 2015. Investigation of the predictability and physical mechanisms of an extreme-rainfall-producing mesoscale convective system along the Meiyu front in East China: An ensemble approach. Journal of Geophysical Research Atmospheres, 120(20): 10593–10618.

Malinovic-Milicevic S, Radovanovic M M, Stanojevic G, et al. 2016. Recent changes in Serbian climate extreme indices from 1961 to 2010. Theoretical and Applied Climatology, 124: 1089–1098.

Miao C Y, Sun Q H, Duan Q Y, et al. 2016. Joint analysis of changes in temperature and precipitation on the Loess Plateau during the period 1961–2011. Climate Dynamics, 47(9–10): 3221–3234.

Paul S, Ghosh S, Mathew M, et al. 2018. Increased spatial variability and intensification of extreme monsoon rainfall due to urbanization. Scientific Reports, 8: 3918, doi: 10.1038/s41598-018- 22322-9.

Peterse F, Prins M A, Beets C J, et al. 2011. Decoupled warming and monsoon precipitation in East Asia over the last deglaciation. Earth and Planetary Science Letters, 301(1–2): 256–264.

Sillmann J, Kharin V V, Zhang X, et al. 2013. Climate extremes indices in the CMIP5 multimodel ensemble: Part 1. Model evaluation in the present climate. Journal of Geophysical Research Atmospheres, 118(4): 1716–1733.

Sun C F, Ma Y Y. 2015. Effects of non-linear temperature and precipitation trends on Loess Plateau drought. Quaternary International, 372: 175–179.

Sun Q H, Miao C Y, Duan Q Y, et al. 2015. Temperature and precipitation changes over the Loess Plateau between 1961 and 2011, based on high-density gauge observations. Global and Planetary Change, 132: 1–10.

Torrence C, Compo G P. 1998. A practical guide to wavelet analysis. Bulletin of the American Meteorological Society, 79(1): 61–78.

Wang K B, Deng L, Shangguan Z P, et al. 2021. Sustainability of eco- environment in semi-arid regions: Lessons from the Chinese Loess Plateau. Environmental Science & Policy, 125: 126–134.

Wang L L, Yao W Y, Xiao P Q, et al. 2022. The spatiotemporal characteristics of flow-sediment relationships in a hilly watershed of the Chinese Loess Plateau. International Journal of Environmental Research and Public Health, 19(15): 9089, doi: 10.3390/ijerph19159089.

Wang N, Jiao J Y, Bai L C, et al. 2020. Magnitude of soil erosion in small catchments with different land use patterns under an extreme rainstorm event over the Northern Loess Plateau, China. CATENA, 195: 104780, doi: 10.1016/j.catena.2020.104780.

Wang X H, Wang B T, Xu X Y. 2019. Effects of large-scale climate anomalies on trends in seasonal precipitation over the Loess Plateau of China from 1961 to 2016. Ecological Indicators, 107: 105643, doi: 10.1016/j.ecolind.2019.105643.

Wang X L, Chen H F, Wu Y H, et al. 2010. New techniques for detection and adjustment of shifts in daily precipitation data series. Journal of Applied Meteorology and Climatology, 49(12): 2416–2436.

Wang Y R, Wang X W. 2006. Analysis of the temporal and spatial variation of rainfall in the Loess Plateau of China from April to October. Plateau Meteorology, 25(4): 737–743. (in Chinese)

White R H, Battisti D S, Skok G. 2017. Tracking precipitation events in time and space in gridded observational data. Geophysical Research Letters, 44(16): 8637–8646.

Wu S H, Liu L L, Gao J B, et al. 2019. Integrate risk from climate change in China under global warming of 1.5 and 2.0°C. Earth's Future, 7(12): 1307–1322.

Wu W, Ren L, Wei Y, et al. 2021. Impacts of urbanization on extreme regional precipitation events. Discrete Dynamics in Nature and Society, 5: 1–17.

Wu X S, Guo S L, Yin J B, et al. 2018. On the event-based extreme precipitation across China: Time distribution patterns, trends, and return levels. Journal of Hydrology, 562: 305–317.

Xiao C, Wu P L, Zhang L X, et al. 2016. Robust increase in extreme summer rainfall intensity during the past four decades observed in China. Scientific Reports, 6: 38506, doi: 10.1038/srep38506.

Xu K, Xu B B, Ju J L, et al. 2019. Projection and uncertainty of precipitation extremes in the CMIP5 multimodel ensembles over nine major basins in China. Atmospheric Research, 226: 122–137.

Yang H, Liu M, Wang M, et al. 2022. Projections of extreme precipitation in the middle and upper Yangtze River at 1.5°C and 2°C warming thresholds based on bias correction. Theoretical and Applied Climatology, 147: 1589–1600.

Yang L J, Wang C M, Zhang C M, et al. 2022. Based on remote sensing images to study the occurrence and development of new cut ditch under extreme rainstorm conditions. Chinese Journal of Agricultural Engineering, 38(6): 96–104. (in Chinese)

Yang Y F, Wang B, Wang G L, et al. 2019. Ecological zoning and overview of the Loess Plateau. Journal of Ecology, 39(20): 7389–7397. (in Chinese)

Yao J Q, Chen Y N, Chen J, et al. 2020. Intensification of extreme precipitation in arid Central Asia. Journal of Hydrology, 598: 125760, doi: 10.1016/j.jhydrol.2020.125760.

Yao W Y, Hou S Z, Guo Y, et al. 2018. Analysis of the causes of disasters caused by the "7•26" rainstorm in the urban areas of Suide and Zizhou in northern Shaanxi. China Flood Control and Drought Relief, 28: 27–32. (in Chinese)

Zaman M, Ahmad I, Usman M, et al. 2020. Event-based time distribution patterns, return levels, and their trends of extreme precipitation across Indus basin. Water, 12: 3373, doi: 10.3390/w12123373.

Zhang B Q, Shao R, Zhao X N, et al. 2020. The impact of large-scale vegetation restoration on the ecological and hydrological processes of the Loess Plateau. Journal of Applied Basic and Engineering Sciences, 28(3): 594–606. (in Chinese)

Zhao G J, Zhai J Q, Tian P, et al. 2018. Variations in extreme precipitation on the Loess Plateau using a high-resolution dataset and their linkages with atmospheric circulation indices. Theoretical and Applied Climatology, 133: 1235–1247.